Reference: *Biol. Bull.* **199:** 287–297. (December 2000)

Cellular Basis of Gastrulation in the Sand Dollar *Scaphechinus mirabilis*

TETSUYA KOMINAMI* AND HIROMI TAKATA

Department of Biology and Earth Sciences, Faculty of Science, Ehime University, 2-5 Bunkyo-Cho, Matsuyama, 790-8577, Japan

Abstract. The processes of gastrulation in the sand dollar *Scaphechinus mirabilis* are quite different from those in regular echinoids. In this study, we explored the cellular basis of gastrulation in this species with several methods. Cell-tracing experiments revealed that the prospective endodermal cells were convoluted throughout the invagination processes. Histological observation showed that the ectodermal layer remained thickened, and the vegetal cells retained an elongated shape until the last step of invagination. Further, most of the vegetal ectodermal cells were skewed or distorted. Wedge-shaped cells were common in the vegetal ectoderm, especially at the subequatorial region. In these embryos, unlike the embryos of regular echinoids, secondary mesenchyme cells did not seem to exert the force to pull up the archenteron toward the inner surface of the apical plate. In fact, the archenteron cells were not stretched along the axis of elongation and were in close contact with each other. Here we found that gastrulation was completely blocked when the embryos were attached to a glass dish coated with poly-L-lysine, in which the movement of the ectodermal layer was inhibited. These results suggest that a force generated by the thickened ectoderm, rather than rearrangement of the archenteron cells, may play a key role in the archenteron elongation in *S. mirabilis* embryos.

Introduction

The processes of gastrulation in sea urchin embryos have been divided into two phases, known as primary and secondary invagination (Dan and Okazaki, 1956; Gustafson and Kinnander, 1956). During primary invagination, the thickened vegetal plate buckles into the blastocoel and gives rise to a short stub-like gut rudiment. After a couple of hours, the gut rudiment begins to elongate, and its tip reaches the inner wall of the apical plate. After secondary invagination, the gut rudiment results in a slender tube-like archenteron.

Primary invagination is autonomous, because the excised vegetal plate can still undergo morphological changes similar to those in the intact embryo (Moore and Burt, 1939; Ettensohn, 1984). One of the driving forces for primary invagination seems to be generated by bottle cells (Nakajima and Burke, 1996; Kimberly and Hardin, 1998). Wedge-shaped cells, which are frequently observed in the vegetal ectodermal layer, may produce another motive force for primary invagination (Burke *et al.*, 1991). During secondary invagination, a population of secondary mesenchyme cells (SMCs) connect the archenteron tip to the inner surface of the apical plate and exert the force to pull up the archenteron (Dan and Okazaki, 1956; Hardin, 1988). Rearrangement of the archenteron cells is an important cellular basis for elongation of the gut rudiment (Ettensohn, 1985; Hardin and Cheng, 1986; Hardin, 1989).

However, these mechanisms apply mainly to the regular echinoids and cannot fully explain the processes of gastrulation in a variety of sea urchins (Ettensohn, 1999). The embryos of a primitive sea urchin, *Eucidaris tribuloides*, show a different manner of gastrulation (Schroeder, 1981; Hardin, 1989); SMCs are not formed, but the embryos gastrulate. Even in the so-called "Regularia," some species of embryos do not show a typical manner of gastrulation (Amemiya *et al.*, 1982a, b). In a previous study, we indicated that the processes of gastrulation in the sand dollar *Scaphechinus mirabilis* (Clypeasteroida) were different from those reported in regular echinoids (Kominami and Masui, 1996). The processes of gastrulation could not be divided into two phases, because invagination proceeded at

Received 9 September 1999; accepted 10 August 2000.

* To whom correspondence should be addressed. E-mail: tkom@sci.ehime-u.ac.jp

a constant rate from beginning to end. Unlike the SMCs of regular echinoids, those of *S. mirabilis* did not form long filopodia. Moreover, the number of archenteron cells observed in cross sections remained unchanged, suggesting the absence of cell rearrangement in the archenteron.

One of the ways to a full understanding of the mechanisms of gastrulation in a species is to study the processes of gastrulation in a variety of related species. A less important factor in one species may be crucial in another species. The purpose of this study is to elucidate the cellular basis of gastrulation in *S. mirabilis* embryos. Changes in the morphology of gastrulating embryos were quantified. To clarify the movements of vegetal cells during gastrulation, cell-tracing experiment was undertaken. The shapes of constituent cells were observed on scanning electron micrographs and in immunostained specimens. To examine whether the ectodermal layer plays a role in archenteron elongation, the movement of the layer was inhibited by attaching the embryos to a glass dish coated with poly-L-lysine. Some of the results are compared with those obtained in the sea urchin *Hemicentrotus pulcherrimus* (Echinida), which shows a typical pattern of sea urchin gastrulation.

Materials and Methods

Animals

Adults of the sand dollar *Scaphechinus mirabilis* and the sea urchin *Hemicentrotus pulcherrimus* were collected and kept in aquaria supplied with circulating cold seawater (18°C for *S. mirabilis* and 15°C for *H. pulcherrimus*). Gametes of both species were handled as previously described (Kominami and Masui, 1996). Millipore-filtered seawater (MFSW) supplemented with 100 units/ml penicillin and 50 μg/ml streptomycin (Meiji Seika, Tokyo) was used throughout the experiments. Embryos of both species were cultured at 18 ± 1°C.

Histological observation

Gastrulating embryos were fixed with 1% glutaraldehyde dissolved in MFSW at room temperature for 2 h. After two rinses with MFSW, an aliquot of fixed embryos was dehydrated with an acetone series and mixed with Spurr resin. A drop of the mixture was mounted on a glass slide, sealed with coverslips, and polymerized. These specimens were for measurements of the thickness of the blastocoel wall, which cannot be obtained accurately in living embryos, because of optical reflections through the ectodermal layer.

Another aliquot of specimens was post-fixed with 1% OsO_4 dissolved in MFSW for 1 hr. The embryos were dehydrated with an ethanol series and critical-point dried (Hitachi, HCP-1, Tokyo). The specimens were adhered to the stub with a piece of double-sided transparent tape, and were fractured with a fine tungsten needle under a dissecting microscope. These specimens were coated with gold and platinum (Eiko, IB-3, Tokyo), and observed under a scanning electron microscope (Hitachi, S-450DX).

Cell contours were traced on scanning electron micrographs using transparent sheets. Shapes of cells were classified into four types according to the criteria described in Burke *et al.* (1991): columnar, cells longer than wide and rectangular in outline; wedge-shaped, apical surface broader than basal surface; skewed, the apex of the cell deviates from the apical basal axis; and others. The frequency of the appearance of these types of cells was obtained by examining between 4 and 19 SEM images at each observation point. Degree of archenteron invagination was obtained according to the method described in the previous report (Kominami and Masui, 1996). More than 20 embryos were measured at each observation point.

Cell tracing

The vegetal blastomeres of the 8-cell-stage embryos of *S. mirabilis* were somewhat smaller than those in the animal hemisphere. This morphological characteristic was used to orient the 8-cell-stage embryos so that Lucifer yellow CH (Sigma, St. Louis, MO) could be injected into one of the vegetal blastomeres. An experimental setup for iontophoretic injection of the dye was previously described (Kominami, 1988). The dye-injected embryos were observed under an epifluorescence microscope (Olympus, BH-RFL, Tokyo), and photographed.

Immunofluorescence

Gastrulating embryos were fixed successively with cold methanol and ethanol (−20°C), 20 min in each. Fixed embryos were embedded in polyester wax (BDH Laboratory Supplies, Poole, England) and sectioned (6 μm). After removal of the wax with absolute ethanol, specimens were rinsed twice with phosphate-buffered saline (PBS), and were reacted with a monoclonal antibody (VE10) that recognizes the carbohydrates at the cell surface. After the primary reaction, the specimens were rinsed twice with PBS, and then reacted with FITC-conjugated goat anti-mouse IgG (Sigma) for 1 h. The immunostained sections were mounted on a glass slide with a small amount of glycerol.

Attaching the embryos to the glass dish

The cleaned glass dish was soaked overnight in 1 mg/ml poly-L-lysine (Sigma) dissolved in distilled water. After the solution was removed, the glass dish was rinsed three times with distilled water and air-dried. A micropipette was used to attach the gastrulating embryos to the bottom of the glass dish; in some cases, the embryos were pressed against the bottom of the dish with a fine glass needle, to ensure

Figure 1. Processes of gastrulation in *Hemicentrotus pulcherrimus* and *Scaphechinus mirabilis*. Embryos of both species were cultured at 18°C and observed hourly. Embryos were embedded in Spurr resin. (A–F) *H. pulcherrimus*, 17–22 h. (G–L) *S. mirabilis*, 14–19 h. In *H. pulcherrimus* embryos, the primary and secondary invagination is clearly distinguished by the presence of a pause in the archenteron elongation (C–D, 1–2 hours). After the occurrence of the secondary invagination, the archenteron became slender. In *S. mirabilis* embryos, the archenteron invaginated continuously, and the diameter of the archenteron remained unchanged during gastrulation. The scale bar indicates 50 μm.

attachment. The processes of gastrulation were photographed at intervals of 10 min.

Results

Morphological changes during gastrulation

Figure 1 shows the processes of gastrulation in embryos of *H. pulcherrimus* (A–F) and *S. mirabilis* (G–L) kept at 18°C. In a regular echinoid, *H. pulcherrimus*, primary (Fig. 1A–C) and secondary invagination (Fig. 1D–F) were clearly distinguished by the presence of a time lag in archenteron elongation (1–2 h, Fig. 1C–D). On the other hand, the archenteron of *S. mirabilis* embryos elongated at a constant rate during the course of invagination (Fig. 1G–L).

Besides archenteron elongation, several differences were noticed in the morphology of the embryos of these two species. In *H. pulcherrimus*, the height of the embryo increased to some extent during primary invagination. After the onset of secondary invagination, the embryos were shortened along the animal-vegetal axis (Fig. 2A). The width of the embryos increased as gastrulation progressed (Fig. 2B). This was caused by the expansion of the ectodermal layer, especially at the lateral blastocoel wall (Fig. 2C). In contrast, *S. mirabilis* embryos became shorter as invagination progressed (Fig. 2D). Though their width increased to some extent (Fig. 2E), the expansion of the ectodermal layer was not so conspicuous as in *H. pulcherrimus* (Fig. 2F).

Tracing of the vegetal blastomeres

The dye-injected *S. mirabilis* embryos were examined to learn how vegetal cells move toward the blastopore during gastrulation (Fig. 3). Before the initiation of invagination, the boundary between labeled and nonlabeled cells was at about 50% of the distance from the vegetal pole to the animal pole (Fig. 3A, A′). The boundary gradually shifted toward the vegetal pole side as invagination progressed (Fig. 3B, B′, C, C′, D, D′). At the end of invagination, the

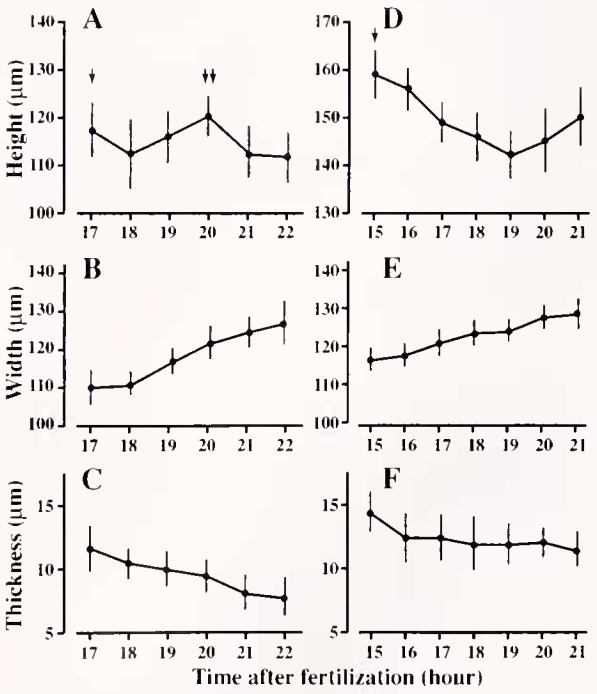

Figure 2. Change in the height and width of the embryos, and in the thickness of the blastocoel wall (the lateral part of the embryo) during gastrulation. (A–C) *Hemicentrotus pulcherrimus*. (D–F) *Scaphechinus mirabilis*. Single arrows indicate the time of the initiation of gastrulation. Double arrows indicate the time of the onset of the secondary invagination in *H. pulcherrimus* embryos. Changes in the height of the embryo (A, D) show different patterns. In both species, the width of the embryo increased as invagination progressed (B, E). This is more evident in *H. pulcherrimus* than in *S. mirabilis*. The thickness of the blastocoel wall decreases during gastrulation, but the change is not conspicuous in *S. mirabilis* (C, F).

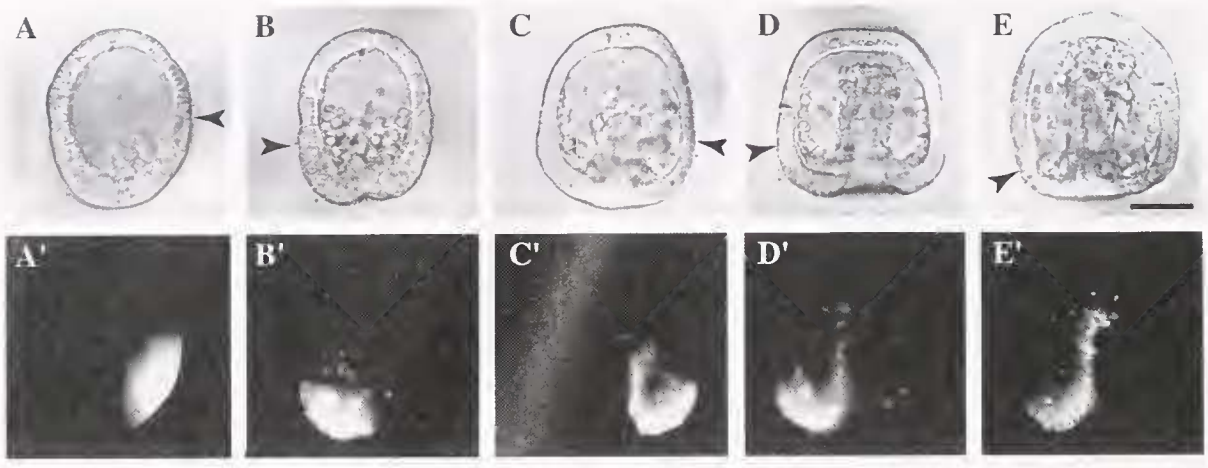

Figure 3. Movement of vegetal cells during gastrulation in *Scaphechinus mirabilis* embryos: bright-field images (A–E); fluorescence images (A′–E′). (A, A′) 14 h. (B, B′) 16 h. (C, C′) 17 h. (D, D′) 18 h. (E, E′) 20 h. Distribution of labeled cells in invaginating gastrulae, which had been injected with Lucifer yellow CH into one of vegetal blastomeres at the 8-cell stage, was examined. As gastrulation proceeds, the boundary between labeled and nonlabeled cells moves downward. Arrowheads in A–E demarcate the boundary observed on fluorescent images. The scale bar indicates 50 μm.

boundary was located at 10%–15% of the embryo length from the vegetal pole (Fig. 3E, E′). This value corresponds to the thickness of the anal plate ectoderm. The relationship between the degree of invagination and the position of the boundary is shown in Figure 4. During the early stages of invagination, the position of the boundary shifted rapidly to the vegetal pole; during the later stages, the rate of the movement decreased gradually. The result clearly indicates that the involution of cells through the blastopore continues until the archenteron tip reaches the apical plate.

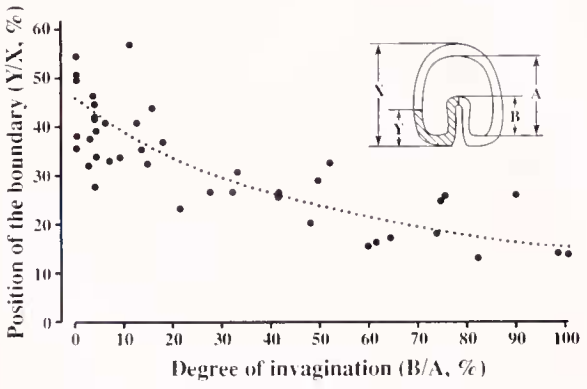

Figure 4. Change in the position of the boundary between animal and vegetal ectoderm during gastrulation. The degree of invagination (%) and the position of the boundary along the embryo axis (%) were sought using the parameters shown in the inset. The most fitting hyperbolic curve is also shown. The movement of the vegetal cells toward the vegetal pole continues throughout the invagination processes, though the rate of the movement changes.

Shapes of the ectodermal cells during early stages of gastrulation

The shapes of the ectodermal cells during early stages of gastrulation were examined with SEM (Fig. 5). The cells were classified as columnar, skewed, wedge-shaped, and other, as described in the Materials and Methods. Among these types, wedge-shaped cells showed differences in their distribution between the two species of embryos. In *H. pulcherrimus,* two to three wedge-shaped cells were observed just at the bending point of the ectodermal epithelium (Fig. 5A–D, arrowheads). In *S. mirabilis,* such wedge-shaped cells were distributed more broadly apart from the blastopore (Fig. 5E–H, arrowheads). In addition, the number of wedge-shaped cells was larger than in *H. pulcherrimus.* At the beginning of invagination, bottle-shaped (apically constricted and basally rounded-up) cells were frequently observed in the bending vegetal plate (arrows indicate bottle cells in Fig. 5D [*H. pulcherrimus*] and 5G [*S. mirabilis*]).

Figure 6 shows the change in the ratio of these three types of cells during early stages of gastrulation. In both species, it takes 3–4 h to give rise to a short, stub-like gut rudiment after the first sign of invagination. These stages were divided hourly and designated Stages I–IV. In the animal halves, columnar and skewed cells were abundant (Fig. 6A, *H. pulcherrimus;* 6C, *S. mirabilis*). In both species, the ratio of columnar cells increased as gastrulation progressed. In contrast, most cells in the vegetal half were skewed or distorted (Fig. 6B, *H. pulcherrimus;* 6D, *S. mirabilis*). In *H. pulcherrimus,* wedge-shaped cells occupied nearly 40% of the total at the initial stage of invagination, but decreased to

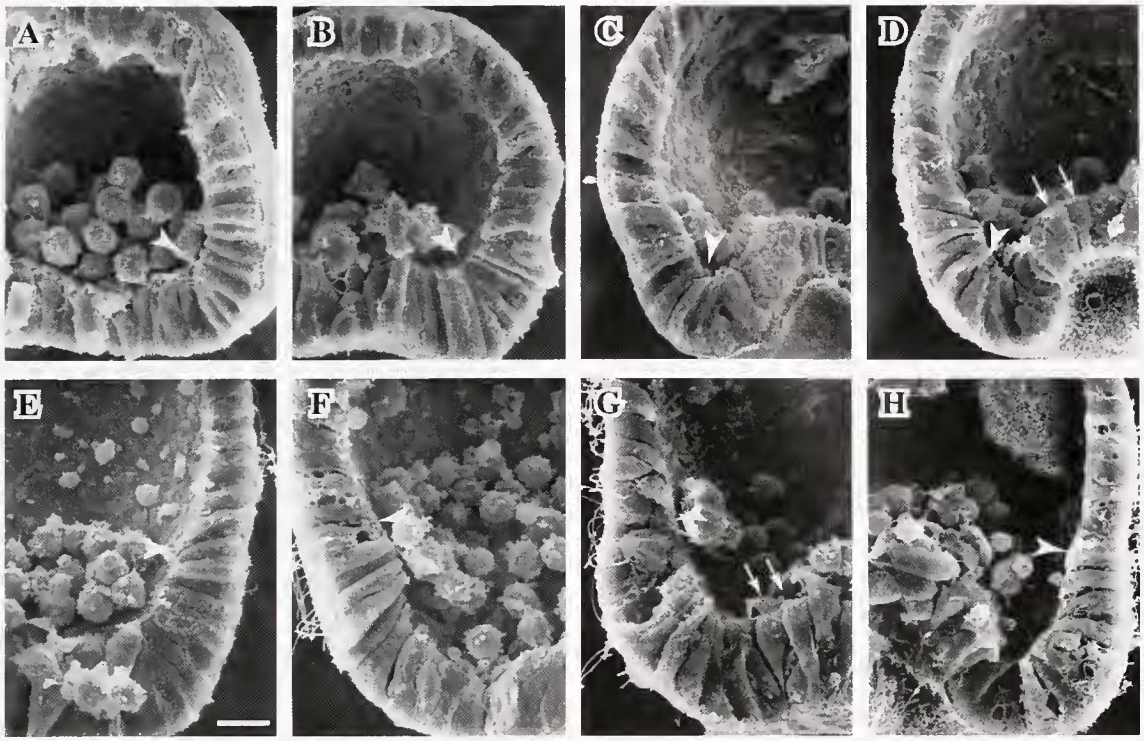

Figure 5. Scanning electron micrographs of the cells in the ectoderm and invaginated archenteron during early stages of gastrulation: *Hemicentrotus pulcherrimus* (A–D); *Scaphechinus mirabilis* (E–H). In A–D, arrowheads indicate the bending point; in E–H they indicate the boundary between animal and vegetal cells. Arrows in D and G indicate bottle cells. Ectodermal cells of *S. mirabilis* (F–H) were more elongated in the apico-basal direction than those of *H. pulcherrimus* (B–D). Columnar and skewed cells were frequently observed in both species. Wedge-shaped cells were also observed in both species, especially in the vegetal half. In *H. pulcherrimus*, two to three wedge-shaped cells were observed just at the bending point of the epithelium (B, C). Such wedge-shaped cells are distributed more broadly apart from the blastopore in *S. mirabilis* (F, G). The scale bar indicates 10 μm.

about 20% as invagination progressed; in *S. mirabilis*, the ratio remained constant at a rather higher level. Columnar cells were barely observed in *S. mirabilis* (Fig. 6D), whereas this type of cell increased in *H. pulcherrimus* at the end of primary invagination (Fig. 6B).

Secondary mesenchyme cells at the archenteron tip

Figure 7 shows the secondary mesenchyme cells observed at the archenteron tip of the midgastrulae. In *H. pulcherrimus*, these cells were globular and formed long thin filopodia. Several SMCs were located between the archenteron tip and the future oral opening region. In *S. mirabilis*, SMCs were flattened to some extent and formed broad ruffled membranes. No cells were observed between the archenteron tip and the future oral opening region. Although more than 200 gastrulating *S. mirabilis* embryos were examined, an image that showed direct contact between the filopodia of the SMCs and the inner surface of the apical plate could not be obtained.

Shape of archenteron cells during later stages of invagination

Figure 8 shows cross fractures of the archenteron at later gastrula stages. SEM images of the archenteron at three levels along its axis (top, middle and bottom) are shown. The cells in the archenteron of *H. pulcherrimus* were cuboid and loosely in contact with each other (Fig. 8A–C). The numbers of cells observed in cross fractures increased from top (6–7) to bottom (about 12) of the archenteron. The archenteron cells had a rounded basal surface. In contrast, cells in the archenteron of *S. mirabilis* embryos were elongated along the apico-basal direction (Fig. 8D–F). The numbers of cells observed in cross fractures were almost the same at the top (14–15), middle (13), and bottom (13) levels of the archenteron.

As gastrulation proceeded, it became difficult to crack the archenteron along its long axis. The shapes of cells in the embryos at later stages of invagination were examined on histological sections. The stages shown in Figure 9 correspond to the secondary invagination in *H. pulcherrimus* embryos. As clearly shown, the cells in the archenteron of

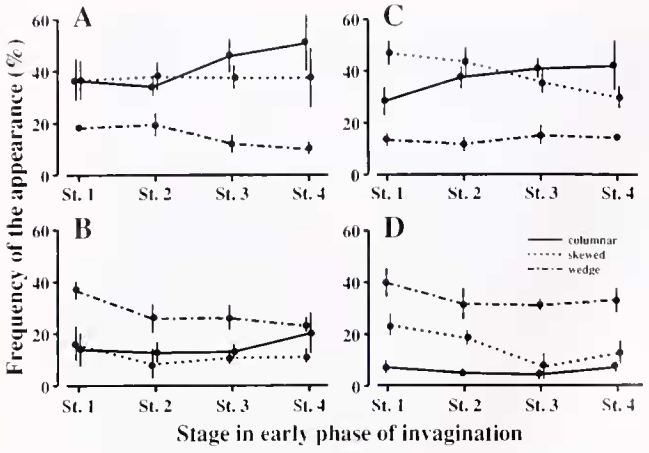

Figure 6. Frequency of the appearance of columnar, skewed, and wedge-shaped cells during gastrulation: *Hemicentrotus pulcherrimus* (A, B); *Scaphechinus mirabilis* (C, D). (A, C) Animal hemisphere. (B, D) Vegetal hemisphere. Columnar cells (solid lines) are more abundant in the animal hemisphere. Skewed cells (dotted lines) were observed more frequently in *S. mirabilis*. In both species, the population of columnar cells increased as the gastrulation proceeded (A, C). Wedge-shaped cells (broken lines) appear sparsely in the animal hemisphere. In contrast, the most abundant type of cells are wedge-shaped cells in the vegetal halves (B, D). Columnar cells were rarely observed in *S. mirabilis*, but such cells increased in *H. pulcherrimus* after the secondary invagination had started.

H. pulcherrimus embryos were stretched along the axis of the archenteron (Fig. 9A–D). After the completion of the secondary invagination, the cells resumed a cuboid shape (Fig. 9E–F). In contrast, the cells in the archenteron of *S. mirabilis* embryos were not stretched at any stage of later invagination (Fig. 9G–L). It should be noted that the cells near the blastopore were elongated along their apico-basal direction through all the stages examined.

These changes in cell shape were quantified according to the methods described by Hardin (1988); two ratios, *Y/X* (ratio of lengths along and perpendicular to the axis of the archenteron) and *L/W* (ratio of cell length and width) were obtained (Fig. 10). Both *Y/X* and *L/W* increased during the secondary invagination in *H. pulcherrimus* embryos, and decreased to the initial level at the end of secondary invagination (Fig. 10A). On the other hand, the ratios did not change in *S. mirabilis* embryos through these stages of invagination (Fig. 10B). The result clearly shows that the archenteron cells in *S. mirabilis* embryos were not stretched along the axis of the archenteron.

Attaching embryos to a glass dish coated with poly-L-lysine

The obtained results suggest the ectodermal layer plays a role in the invagination process in *S. mirabilis* embryos. If

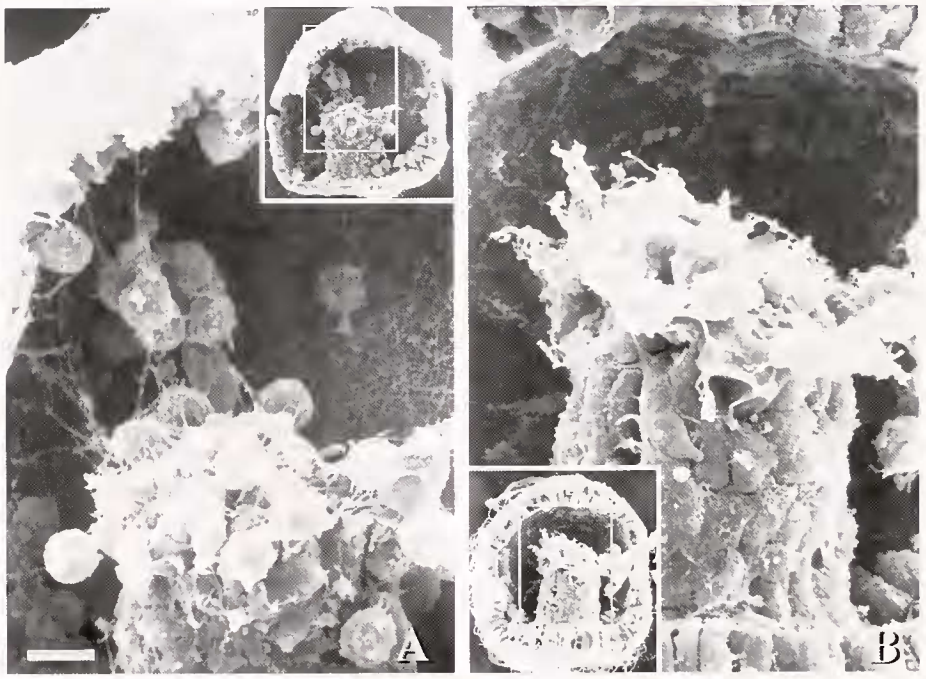

Figure 7. Scanning electron micrographs of the secondary mesenchyme cells at the archenteron tip. *Hemicentrotus pulcherrimus* (A); *Scaphechinus mirabilis* (B). Insets in A and B show whole view of the mid-gastrula. Secondary mesenchyme cells in *H. pulcherrimus* are globular in shape and form long thin filopodia. Several secondary mesenchyme cells (SMCs) are located between the archenteron tip and the inner surface of the future oral opening region. In contrast, SMCs are flattened and form ruffled membranes in *S. mirabilis* gastrulae. No SMCs were observed between the archenteron tip and the future oral opening region. The scale bar indicates 10 μm.

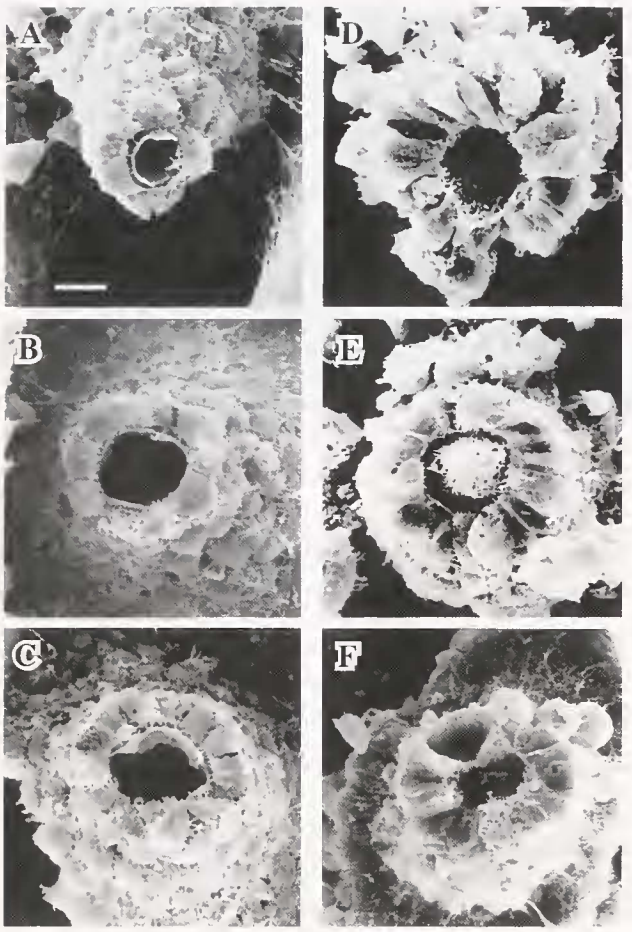

Figure 8. Scanning electron micrographs of the cells in the archenteron after the completion of invagination: *Hemicentrotus pulcherrimus* (A–C); *Scaphechinus mirabilis* (D–F). Top (A, D), middle (B, E), and bottom (C, F) levels of the archenteron are shown. The cells in the archenteron of *H. pulcherrimus* are cuboid, while those in *S. mirabilis* are elongated along the apico-basal direction. Note that the wall of the archenteron is thicker in *S. mirabilis* than in *H. pulcherrimus*. The scale bar indicates 10 μm.

this is the case, immobilization of the ectodermal layer should affect the invagination process. To test this possibility, the change in the length of the archenteron was monitored in gastrulating embryos attached to a glass dish coated with poly-L-lysine.

H. pulcherrimus gastrulae attached to the poly-L-lysine coated glass dish (Fig. 11A). If the embryos had been undergoing primary invagination when attached, the invagination was slowed and tip of the archenteron could not reach the apical plate. However, the embryos gastrulated almost normally if they had been attached after primary invagination. In these cases, the rate of archenteron elongation was not different from that in control embryos (Fig. 11B).

In contrast, the invagination process was greatly affected in *S. mirabilis* embryos. If the embryos were not pressed against the bottom of the glass dish using a glass needle, they did not firmly attach to the glass dish. Embryo II shown in Figure 12 loosely attached to the glass dish, so that its position changed during observation. In this embryo, invagination occurred almost normally. On the other hand, embryos I, III, and IV were rather firmly attached to the glass dish. In these embryos, invagination of the gut rudiment was considerably delayed. Nonetheless, embryos III and IV restarted invagination when they detached from the glass dish (Fig. 12F and H, respectively). Embryos that were firmly attached to the glass dish could not gastrulate at all, irrespective of the degree of invagination at attachment (Fig. 13A and B). In addition, the contour of the embryos was distorted during prolonged observation.

Discussion

Involution of the vegetal cells continues during gastrulation

Endodermal tissue in sea urchin embryos had been thought to be exclusively derived from the veg_2 tier of blastomeres formed at the 60-cell stage (Hörstadius, 1973; Cameron *et al.*, 1987, 1991; Ruffins and Ettensohn, 1996). More recently, it has been shown that the descendants of the veg_1 tier of blastomeres also participate in the formation of the digestive tract (McClay and Logan, 1996; Logan and McClay, 1997). The recruitment of the veg_1-derived cells seems to occur only after the tip of the archenteron reaches the apical plate (Martins *et al.*, 1998; Piston *et al.*, 1998; Ransick and Davidson, 1998). The mechanisms of such late ingression of endodermal cells are, however, unknown. Here we focus on the invagination processes that occur before and around the time that the archenteron tip reaches the inner surface of the apical plate.

In embryos of an irregular echinoid, *S. mirabilis*, some unique aspects of gastrulation were elucidated from the measurement of the size of the gastrulating embryos. As is well known, the embryos of regular echinoids expand considerably during gastrulation (Fig. 1A–F). This expansion was caused by thinning of the ectoderm (Fig. 2C). In contrast, the thinning of the blastocoel wall was not so conspicuous in *S. mirabilis* (Fig. 2F). Although the width of the embryos became somewhat larger, their height became smaller as invagination progressed (Fig. 1G–L). This implies a physical continuity between endodermal and ectodermal epithelia during invagination. In fact, convolution of the vegetal cells continued until the archenteron tip reached the apical plate (Figs. 3, 4), whereas such convolution terminates at the end of primary invagination in regular echinoids (Burke *et al.*, 1991).

In *H. pulcherrimus* embryos, invagination was partially inhibited if the embryos just undergoing primary invagination were attached to a glass dish coated with poly-L-lysine (Fig. 11, embryos III and IV). However, the archenteron elongated almost normally if the embryos

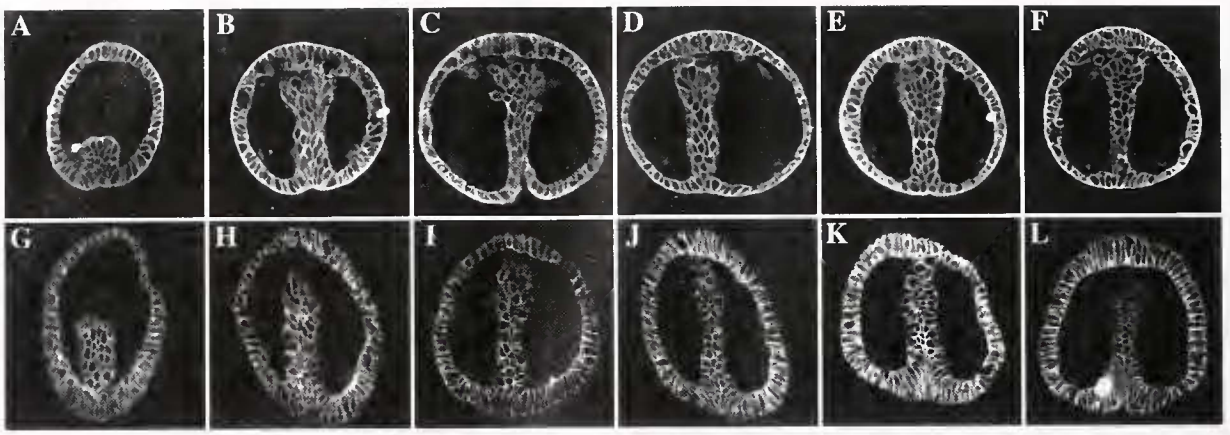

Figure 9. Change in the contour of cells during later stages of invagination as seen in immunostained histological sections. (A–F) *Hemicentrotus pulcherrimus* embryos at 19, 20, 22, 24, 26, and 28 h, respectively. (G–L) *Scaphechinus mirabilis* embryos at 17, 18, 19, 20, 21, and 22 h, respectively. The ectodermal cells in *H. pulcherrimus* embryos were initially elongated along the apico-basal direction (A), and became cuboid with the progress of gastrulation. The archenteron cells were stretched along the axis of the archenteron (B–D or E), and resumed a cuboid shape (F). In contrast, both the ectodermal and endodermal cells in *S. mirabilis* embryos remained elongated along the apico-basal direction during the later stages of invagination (G–L).

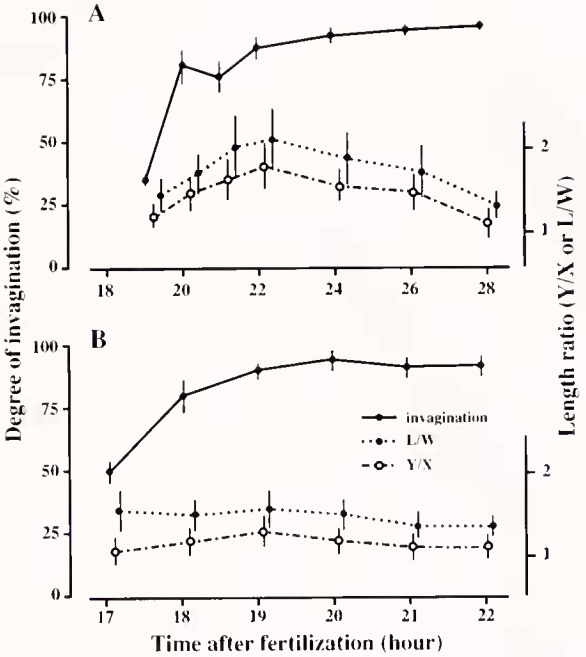

Figure 10. Change in the shape of the archenteron cells during later stages of gastrulation: *Hemicentrotus pulcherrimus* (A); *Scaphechinus mirabilis* (B). Shape was expressed as two ratios: *Y/X* (length along the archenteron axis to length perpendicular to the axis) and *L/W* (cell length to width). In *H. pulcherrimus* embryos, both ratios increased as secondary invagination progressed, up to at least 22 h. Then the ratios decreased to about 1.0. In *S. mirabilis* embryos, the ratios did not change significantly, though the degree of invagination increased. The *Y/X* ratio remained about 1.0, which indicates that the archenteron cells are not stretched along the axis of the archenteron.

had finished primary invagination when attached (Fig. 11, embryos I and II). This suggests that the vegetal ectodermal layer moves toward the blastopore during primary invagination, and that the layer loses physical continuity from the gut rudiment after the completion of primary invagination. On the other hand, elongation of the archenteron was completely blocked in *S. mirabilis* if the embryos were attached to a coated glass dish, irrespective of the degree of invagination (Fig. 13). This inhibitory effect of poly-L-lysine cannot be ascribed solely to the chemical toxicity of the drug, because the embryos restarted gastrulation soon after they detached from the glass dish (Fig. 12). We suppose that the ectodermal epithelium and the invaginated archenteron are physically continuous during the invagination processes and that the blockage of invagination is mainly due to physical constraint of the ectodermal layer attached to the glass dish.

The precise mechanism by which elongation of the gut rudiment is blocked in *S. mirabilis* embryos is unknown. The ectodermal layer seems to be more rigid in *S. mirabilis* embryos than in those of *H. pulcherrimus*, because the former is thicker (Fig. 2F). In addition, *S. mirabilis* embryos retained normal configuration after they were fixed with 10% formaline, while the ectodermal layer of *H. pulcherrimus* embryos was severely distorted when the fixative was applied. The ectodermal cells in *S. mirabilis* embryos are probably tightly connected with each other, forming a rigid structure over the entire vegetal ectoderm. Even if embryos are attached to the glass dish on one side of the body, such a rigid structure may be destroyed totally, resulting in a blockage of archenteron elongation.

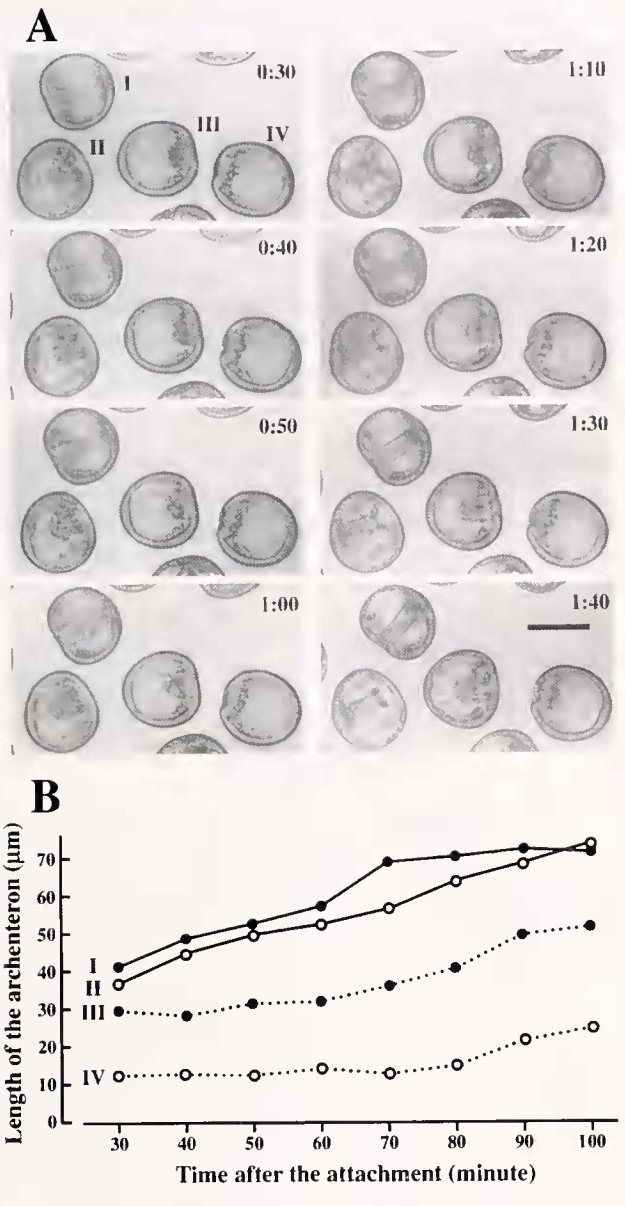

Figure 11. Adhesion of *Hemicentrotus pulcherrimus* embryos to the glass dish coated with poly-L-lysine. The numeral at the top right corner in each photograph in A indicates the time after the attachment to the glass dish. Roman numerals (I–IV) in A and B indicate the same embryos. The embryos gastrulated almost normally if they had been attached after the primary invagination (embryo I and II). If the embryos had been just in the primary invagination when attached, the rate of elongation of the archenteron was slowed and the archenteron could not reach the apical plate (embryo III and IV). The scale bar indicates 100 μm.

The initial phase of gastrulation

In both species of embryos, bottle cells (Nakajima and Burke, 1996) were observed in the vegetal plate (Fig. 5D, G, arrows). The appearance of bottle cells in the vegetal plate may lead to the first step of invagination, if the archenteron cells retain the monolayer arrangement (Gustafson and Wolpert, 1963, 1967). Unlike the archenteron cells in *H. pulcherrimus* embryos (Fig. 5C, D), those in *S. mirabilis* embryos were variable in shape and were not organized into a complete monolayer sheet (Fig. 5G, H). As a result, the force produced by bottle cells does not necessarily cause the bending of the vegetal plate. Other forces seem to be necessary to produce the invagination of the vegetal plate cells in *S. mirabilis* embryos.

In this study, several types of cells were observed on SEM images. The role of each type of cell is unknown. If cells are pulled apically or basally, they should become skewed, because cells are connected with extracellular matrix (Wessel and McClay, 1987; Burke *et al.*, 1991; Berg *et al.*, 1996). If a monolayer cell sheet is bent, wedge-shaped cells should appear at the bending point. Thus, the shapes of cells are signs of the existence of the forces generated by surrounding tissues or by the cells themselves. In both species of embryos, the ratio of columnar cells in the animal hemisphere increased as invagination progressed (Fig. 6A, C). On the other hand, most cells in the vegetal hemisphere were distorted (Fig. 6B, D). Especially in *S. mirabilis* embryos, columnar cells were barely observed through the stages examined. These results imply that

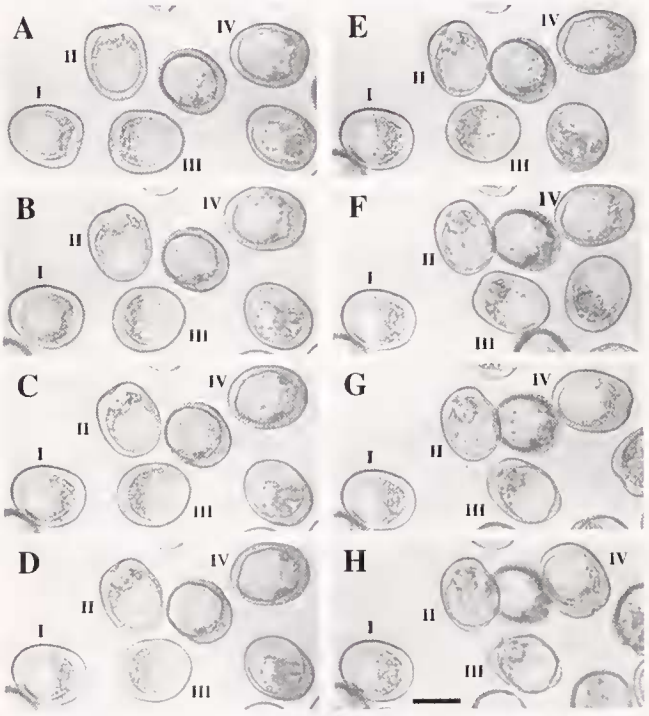

Figure 12. Adhesion of the *Scaphechinus mirabilis* embryos to the glass dish coated with poly-L-lysine. Embryo II was loosely attached to the glass dish, because its position changed during observation. In this embryo, invagination occurred almost normally. On the other hand, embryos I, III, and IV were rather firmly attached to the glass dish and invagination of the gut rudiment were considerably delayed. Nonetheless, embryos III and IV reinitiated invagination when they detached from the glass dish. The scale bar indicates 100 μm.

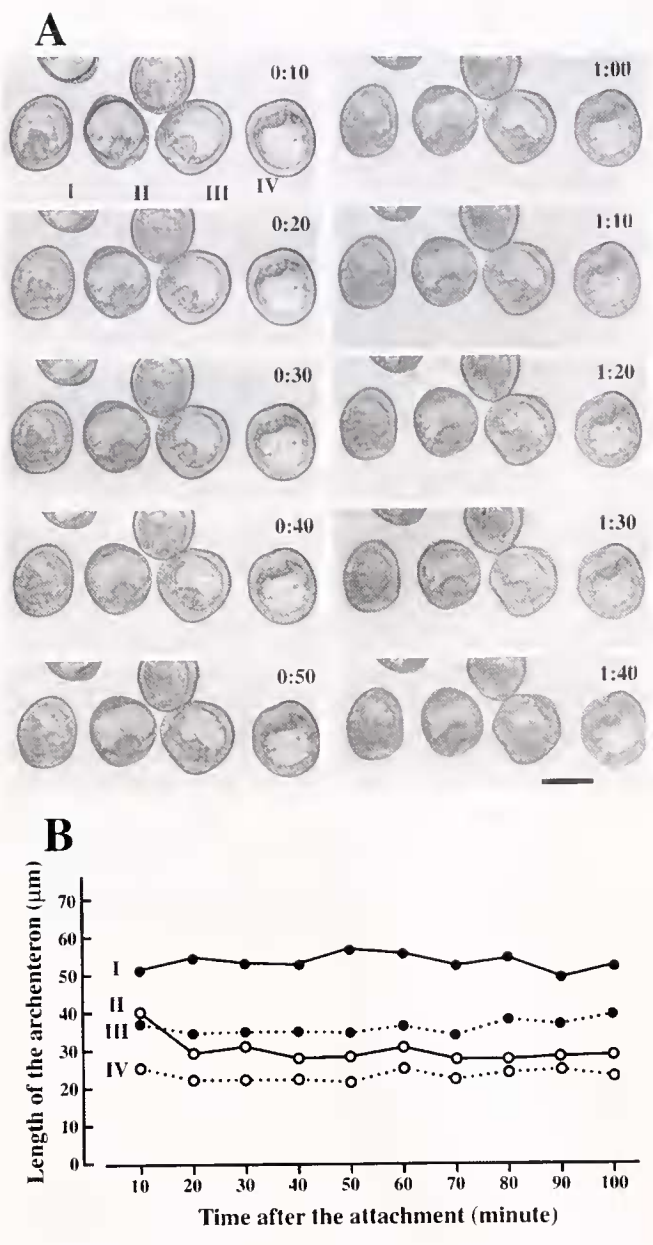

Figure 13. Adhesion of the *Scaphechinus mirabilis* embryos to the glass dish coated with poly-L-lysine. The numeral at the top right corner in each photograph in A indicates the time after the attachment to the glass dish. Roman numerals (I–IV) in A and B indicate the same embryos. *S. mirabilis* embryos could not gastrulate at all, irrespective of the degree of invagination. The scale bar indicates 100 μm.

some forces continue to operate in the vegetal hemisphere of *S. mirabilis* embryos.

Elongation of the archenteron

It is well-established that SMCs pull up the gut rudiment during secondary invagination in some sea urchins (Dan and Okazaki, 1956; Gustafson and Kinnander, 1956; Hardin, 1988; Hardin and McClay, 1990). In *H. pulcherrimus* embryos, a chain of SMCs was observed to connect the archenteron tip and the apical plate (Fig. 7A). The height of the embryos became shortened after the onset of secondary invagination (Fig. 2A). This shortening could be caused by contraction of the SMCs' pseudopodia, which connect the archenteron tip and the apical plate across the blastocoel. The contraction of pseudopodia should stretch the archenteron. In fact, the archenteron cells in *H. pulcherrimus* embryos were stretched along the axis of the archenteron during secondary invagination (Fig. 9B–D, Fig. 10A). On the other hand, the SMCs of *S. mirabilis* embryos did not connect the archenteron tip and the site of the future oral opening (Fig. 7B). Although it is possible that the connecting filopodia were broken by fixation, the archenteron cells in *S. mirabilis* embryos were not stretched throughout the invagination processes (Fig. 9G–L, Fig. 10B). Thus, unlike the SMCs in regular echinoids, those in *S. mirabilis* embryos may not pull up the archenteron.

Rearrangement of archenteron cells is another cellular basis of the extension of the gut rudiment during secondary invagination (Ettensohn, 1985; Hardin and Cheng, 1986; Hardin, 1989). The archenteron cells of *H. pulcherrimus* embryos were cuboid, with rounded basal surfaces (Fig. 8A–C). In contrast, the archenteron cells in *S. mirabilis* embryos were elongated—a configuration that should be brought about by close contact between cells. In fact, the archenteron cells of *S. mirabilis* embryos looked closely compacted (Fig. 7B). It is unlikely that these cells change their position freely in the archenteron. Moreover, the numbers of cells observed in the cross fractures of the archenteron were almost the same at any level along the axis of the archenteron (Fig. 8D–F). Thus, rearrangement of the archenteron cells is not a major cellular basis of archenteron elongation in *S. mirabilis*.

Motive force for the elongation of the archenteron

During the early stages of invagination, prospective endodermal cells are elongated and concentrated in the vegetal plate in both species of embryos. This configuration of cells may be brought about by an increase in cell adhesiveness or by lateral pressure generated by the surrounding tissues. In *S. mirabilis* embryos, cells near the blastopore were elongated throughout the invagination processes (Fig. 9G–L). On the other hand, vegetal cells regained cuboid shape after the completion of primary invagination in *H. pulcherrimus* (Fig. 9A–F). The archenteron cells in *S. mirabilis* embryos were also elongated along the apico-basal direction (Fig. 8, 9). These cell shapes suggest the existence of the lateral pressure in the thickened vegetal plate and the archenteron.

Wedge-shaped cells observed in the thickened vegetal ectoderm are one possible source of such pressure. Appear-

ance of the wedge-shaped cell in a monolayer cell sheet should produce a bending force, although such a shape of cells is merely a result of a bending of the cell sheet. In both species of embryos, wedge-shaped cells appeared in the thickened vegetal plate prior to invagination (Fig. 5A, E). It should be noted that a mass of wedge-shaped cells is found at the subequatorial region (corresponds to the boundary between the descendants of an_2 and veg_1) in *S. mirabilis* embryos, but is located just at the bending point (boundary between veg_1 and veg_2) around the vegetal plate in *H. pulcherrimus*. Wedge-shaped cells should be formed by constriction of the basally distributed microfilaments. Microfilaments play a key role in generating the motive force for invagination (Lane *et al.*, 1993; Nakajima and Burke, 1996), whereas the elongation of the archenteron is independent of microtubules (Hardin, 1987). The precise distribution of microfilaments, especially in wedge-shaped cells, remains to be examined in *S. mirabilis* embryos.

Acknowledgments

We thank the staff of Tateyama Marine Biological Laboratory for collecting animals and for their hospitality.

Literature Cited

Amemiya, S., K. Akasaka, and H. Terayama. 1982a. Scanning electron microscopy of gastrulation in a sea urchin (*Anthocidaris crassispina*). *J. Embryol. Exp. Morphol.* **67:** 27–35.

Amemiya, S., K. Akasaka, and H. Terayama. 1982b. Scanning electron microscopical observation on the early morphogenetic processes in developing sea urchin embryos. *Cell Differ.* **11:** 291–293.

Berg, L. K., S. W. Chen, and G. M. Wessel. 1996. An extracellular matrix molecule that is selectively expressed during development is important for gastrulation in the sea urchin embryo. *Development* **122:** 703–713.

Burke, R. D., R. L. Myers, T. L. Sexton, and C. Jackson. 1991. Cell movements during the initial phase of gastrulation in the sea urchin embryo. *Dev. Biol.* **146:** 542–557.

Cameron, R. A., B. R. Hough-Evans, R. J. Britten, and E. H. Davidson. 1987. Lineage and fate of each blastomere of the eight-cell sea urchin embryo. *Genes Dev.* **1:** 75–84.

Cameron, R. A., S. Fraser, R. J. Britten, and E. H. Davidson. 1991. Macromere cell fates during sea urchin development. *Development* **113:** 1085–1091.

Dan, K., and K. Okazaki. 1956. Cyto-embryological studies of sea urchins. III. Role of the secondary mesenchyme cells in the formation of the primitive gut in sea urchin larvae. *Biol. Bull.* **110:** 29–42.

Ettensohn, C. A. 1984. Primary invagination of the vegetal plate during sea urchin gastrulation. *Am. Zool.* **24:** 571–588.

Ettensohn, C. A. 1985. Gastrulation in the sea urchin embryo is accompanied by the rearrangement of invaginating epithelial cells. *Dev. Biol.* **112:** 383–390.

Ettensohn, C. A. 1999. Cell movement in the sea urchin embryo. *Curr. Opin. Genet. Dev.* **9:** 461–465.

Gustafson, T., and H. Kinnander. 1956. Micro-aquaria for time-lapse cinematographic studies of morphogenesis in swimming larvae and observation on gastrulation. *Exp. Cell Res.* **11:** 36–51.

Gustafson, T., and L. Wolpert. 1963. The cellular basis of morphogenesis and sea urchin development. *Int. Rev. Cytol.* **15:** 139–214.

Gustafson, T., and L. Wolpert. 1967. Cellular movement and cell contact in sea urchin morphogenesis. *Biol. Rev. Camb. Philos. Soc.* **42:** 442–498.

Hardin, J. D. 1987. Archenteron elongation in the sea urchin embryo is a microtubule-independent process. *Dev. Biol.* **121:** 253–262.

Hardin, J. D. 1988. The role of secondary mesenchyme cells during sea urchin gastrulation studied by laser ablation. *Development* **103:** 317–324.

Hardin, J. D. 1989. Local shifts in position and polarized motility drive cell rearrangement during sea urchin gastrulation. *Dev. Biol.* **136:** 430–445.

Hardin, J. D., and L. Y. Cheng. 1986. The mechanisms and mechanics of archenteron elongation during sea urchin gastrulation. *Dev. Biol.* **115:** 490–501.

Hardin, J. D., and D. R. McClay. 1990. Target recognition by the archenteron during sea urchin gastrulation. *Dev. Biol.* **142:** 86–102.

Hörstadius, S. 1973. *Experimental Embryology of Echinoderms.* Clarendon Press, Oxford.

Kimberly, E. L., and J. Hardin. 1998. Bottle cells are required for the initiation of primary invagination in the sea urchin embryo. *Dev. Biol.* **204:** 235–250.

Kominami, T. 1988. Determination of dorso-ventral axis in early embryos of the sea urchin, *Hemicentrotus pulcherrimus*. *Dev. Biol.* **127:** 187–196.

Kominami, T., and M. Masui. 1996. A cyto-embryological study of gastrulation in the sand dollar, *Scaphechinus mirabilis*. *Dev. Growth Differ.* **38:** 129–139.

Lane, M. C., M. A. R. Koehl, F. Wilt, and R. Keller. 1993. A role for regulated secretion of apical extracellular matrix during epithelial invagination in the sea urchin. *Development* **117:** 1049–1060.

Logan, C., and D. R. McClay. 1997. The allocation of early blastomeres to the ectoderm and endoderm is variable in the sea urchin embryo. *Development* **124:** 2213–2223.

Martins, G. G., R. G. Summers, and J. B. Morrill. 1998. Cells are added to the archenteron in the sea urchin *Lytechinus variegatus*. *Dev. Biol.* **198:** 330–342.

McClay, D. R., and C. Y. Logan. 1996. Regulative capacity of the archenteron during gastrulation in the sea urchin. *Development* **122:** 607–616.

Moore, A. R., and A. S. Burt. 1939. On the locus and nature of the forces causing gastrulation in the embryos of *Dendraster excentricus*. *J. Exp. Zool.* **82:** 159–171.

Nakajima, Y., and R. D. Burke. 1996. The initial phase of gastrulation in sea urchins is accompanied by the formation of bottle cells. *Dev. Biol.* **179:** 436–446.

Piston, D. W., R. G. Summers, S. M. Knobel, and J. B. Morrill. 1998. Characterization of involution during sea urchin gastrulation using two-photon excited photorelease and confocal microscopy. *Microsc. Microanal.* **4:** 404–414.

Ransick, A., and E. H. Davidson. 1998. Late specification of veg_1 lineages to endodermal fate in the sea urchin embryo. *Dev. Biol.* **195:** 38–48.

Ruffins, S. W., and C. A. Ettensohn. 1996. A fate map of the vegetal plate of the sea urchin (*Lytechinus variegatus*) mesenchyme blastula. *Development* **122:** 253–263.

Schroeder, T. E. 1981. Development of a "primitive" sea urchin (*Eucidaris tribuloides*): irregularities in the hyaline layer, micromeres, and primary mesenchyme. *Biol. Bull.* **161:** 141–151.

Wessel, G. M., and D. R. McClay. 1987. Gastrulation in the sea urchin embryo requires the deposition of cross-linked collagen within the extracellular matrix. *Dev. Biol.* **121:** 149–165.